Electronic Supplementary Material (ESI) for Green Chemistry

Cleaving C-H bonds with hyperthermal H_2: facile chemistry to cross-link organic molecules under low chemical- and energy-loads

Tomas Trebicky,[a] Patrick Crewdson,[a] Maxim Paliy,[a] Igor Bello,[a] Heng-Yong Nie,[a] Zhi Zheng,[b] Xiaoli L. Fan,[c] Jun Yang,[d] Elizabeth R. Gillies,[e,f] Changyu Tang[g], Hao Liu[g], K.W. Wong[g], W.M. Lau[g,a,e,*]

[a]Surface Science Western, Western University, 999 Collip Circle, London, Ontario N6J 0J3, Canada

[b]Institute of Surface Micro and Nano Materials, Xuchang University, Xuchang, Henan 461000, China

[c]School of Materials Science and Engineering, Northwestern Polytechnical University, Xian 710072, China

[d]Department of Mechanical and Materials Engineering, Western University, London, Ontario N6A 5B7, Canada

[e]Department of Chemistry, Western University, London, Ontario N6A 5B7, Canada

[f]Department of Chemical and Biochemical Engineering, Western University, London, Ontario N6A 5B7, Canada

[g]Chengdu Green Energy and Green Manufacturing Technology R&D Center, Sichuan, China 610207

Supplementary information

Additional examples of applications of HHIC:

(a) Engineering antimicrobial properties via HHIC of PDMAEMA: number of surviving colonies after contact with left: quaternized PDMAEMA on silicon wafer; right: control silicon wafer.

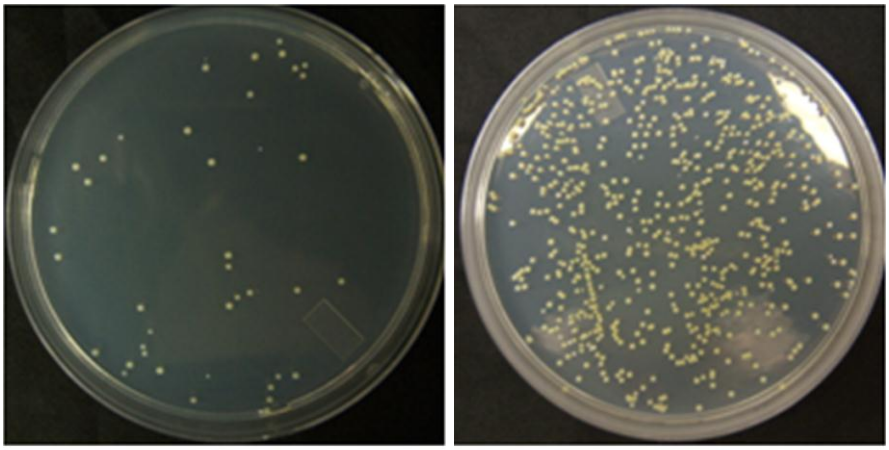

(b) Reducing protein adsorption via HHIC of PEO. Fluorescence confocal microscopy images of the adsorption of a fluorescently labeled fibrinogen on surfaces following HHIC treatment: bottom: PEO on butyl rubber after HHIC and control uncoated butyl rubber.

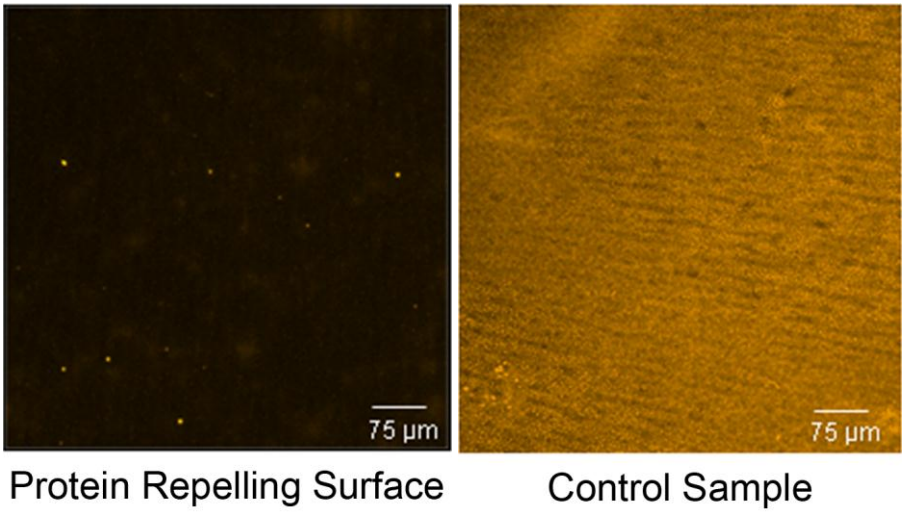

Materials and methods

Polymer curing (cross-linking)

Samples were inserted into a HHIC reactor and pumped down to a background pressure of < $2x10^{-6}$ Torr. Ultra high purity grade hydrogen or helium gas was then introduced inside the reactor until a desired pressure ranging from 0.5 mTorr up to 1.5 mTorr was reached and maintained throughout the experiment. An electron-cyclotron-resonance microwave plasma (2.45 GHz) was set up in a semi-permeable region of the reactor, enclosing the plasma with zero potential. Positive ions were extracted by an applied potential difference ranging from -50 V to -400 V and accelerated into a drift zone, which is a 50 cm long electric field-free region. Residual electrons and positive ions were repelled in two stages with an applied voltage ranging from -50 V to +200 V on respective electrodes. Exposure time and hydrogen ion (or He ion) extraction current were chosen to best suit a given experiment.

The fluence was calculated as follows:

$$fluence = yield \cdot \frac{I_{acc}}{q}\frac{t}{A},$$

where *yield* was obtained from a Monte Carlo simulation described below, I_{acc} is the extraction current, q is the proton charge, t is the exposure time, and A is the effective area of exposure.

Surface analysis by XPS

XPS spectra were recorded by a Kratos AXIS Ultra using a monochromatic Al $K\alpha$ photon source with a beam size of 700 x 300 μm^2. Due to the insulating nature of the materials under study a charge neutralizer was used to supply low energy electrons. Survey scans were collected from 1100 to 0 eV at 160 eV pass energy and 0.5 eV step size for 120 s per sweep. High resolution spectra were collected using a pass energy of 20 eV, a 0.1 eV step size and a 60 s sweep over energy windows ranging from 20 to 40 eV depending on the element studied. Any x-ray beam damage, which is always present in organic polymers in various degrees (1), was not accounted for.

Thickness calculations were carried out using intensities obtained from survey scans following a method developed by Hill *et al.* (2).

Time-of-flight secondary ion mass spectroscopy

An ION-TOF (Gmbh) TOF-SIMS IV equipped with a Bi liquid metal ion gun was employed to investigate the cross-linking of n-$C_{32}H_{66}$ molecules after HHIC. A 25 keV Bi_3^+ cluster primary ion beam with a pulse width of <2 ns (with a target current on the order of 1 pA) was used to bombard the sample surface to generate secondary ions. The positive secondary ions were extracted by an electric field (2 kV) and detected via a reflectron type of time-of-flight analyzer.

A pulsed, low energy electron flood was used to neutralize sample charging. The base pressure of the analytical chamber was around 7×10^{-9} Torr. Spectra were collected from 128 × 128 pixels over an area of 500 μm × 500 μm for 60 s. The mass spectra were calibrated using CH_3^+ and $C_2H_5^+$.

Retention of carboxyl group in PAA

All chemicals ware purchased from commercial suppliers and used as received. A 0.3 wt.% solution was prepared in ethanol. A 70 uL droplet was introduced on freshly cleaned and stripped silicon and subsequently spin-coated at 4000 RPM for 60 s.

The samples were then placed into XPS for chemical analysis before and after HHIC (Fig. 7a). Survey scans and high resolution spectra of C 1s, O 1s and valence band were collected. Although insulating in nature, it was not necessary to supply low energy electrons to compensate for charge imbalance because of the low thickness of the PAA layer.

The PAA layer was then cross-linked in the HHIC reactor at fluence of $6x10^{15}$ cm^{-2}, with accelerating voltage of -96 V.

Efficiency of HHIC as studied on dotriacontane

All chemicals ware purchased from commercial suppliers and used as received. A 0.2 wt.% solution was prepared in heptane. A 70 uL droplet was introduced on freshly cleaved mica and subsequently spin-coated at 1500 RPM for 60 s.

The samples were then placed into XPS for chemical analysis before and after HHIC, as well as after washing. Survey scans and high resolution spectra of C 1s and valence band were collected. Throughout the analysis, the surface of dotriacontane was supplied with low energy electrons to compensate for charge imbalance.

The dotriacontane was then placed inside the HHIC reactor for exposure to hydrogen and helium. The effects and degree of cross-linking were mapped by using different HHIC conditions: fluences ranged from $1x10^{15}$ to $2x10^{17}$ cm^{-2}, accelerating voltages and pressures varied as mentioned above. The experiment comparing the effects of H_2 and He driven HHIC on thickness changes was carried out at a pressure of 1 mTorr with 400 eV extraction energy and fluence of $3x10^{16}$ cm^{-2}. All samples were kept under vacuum if not treated by HHIC.

Dotriacontane samples were washed by spin-casting a 70 uL droplet of heptane at 1500 RPM for 60 s. This step was repeated twice.

Engineering of surface mechanical properties of butyl rubber

Bromobutyl 2030 was heat pressed between Teflon sheets to a thickness of ~5 mm at Lanxess and delivered to SSW. The samples were then cut to appropriate size with no further modifications or preparation and subjected to HHIC. HHIC conditions were -96 V accelerating Voltage, 87.5 mT, 200 W, 0.80 mTorr H_2 using +80 V and -60 V as retarding potentials.

Force-distance curves were collected on the bromobutyl samples using a Dimension V atomic force microscope (AFM) of Veeco Inc. with the Nanoscope V controller. A silicon nitride cantilever having a spring constant of 3 N/m and a tip radius of 10 nm was used in tapping mode to first image an area of 10 µm x 10 µm. If the area was free of debris a box pattern of 25 spots was selected and force-distance curves were measured. All data were fit using a Hertzian model over an indent depth of 20 nm on the portion of the curve corresponding to indentation into the material. The Young's modulus was determined by taking the output of the least squares equation of the Hertzian fit according to the formula:

$$F^2 = \left[\frac{16E_t^2 R}{9\left(1-\upsilon_t^2\right)}\right]^{1/2} \tau^{3/2},$$

where F is the applied force, E_t the Young's modulus of the sample, R the tip radius, υ_t the Poisson's ratio (0.5) of the sample and τ the indent depth. The Young's modulus values for each sample were then averaged and a standard deviation was determined.

Increasing wettability and reducing internal impedance of lithium-ion battery separator via HHIC of PEO

Poly (ethylene oxide) (PEO, molecular weight of 100,000) in chloroform was spin-coated on the surface of a polypropylene (PP) separator (Celgard 2400) to create a thin PEO film. The sample was HHIC-treated for 10-60 seconds. The contact angles of the pristine and cross-linked separator were examined by a contact angle goniometer (JGW-360C, Chenghui Testing Machine Company, China). AC impedance measurements were performed using a CHI660D electrochemical workstation (Shanghai ChenHua instruments Co., Ltd., China) over a frequency range from 0.1 Hz to 100 kHz. The cycling tests at different current densities including 0.1C (C = 274 mAh/g) and 10 C were conducted in the voltage range of 3.0-4.2 V at room temperature using an Arbin multi-function measurement system (BT-2000, Arbin Company, USA).

Engineering of antimicrobial properties

PDMAEMA was prepared as previously reported (3). All chemicals were purchased from commercial suppliers and used as received. Silicon wafers were purchased from Solar Wafer. They were cut into small pieces (approximately 1.5 cm × 1.5 cm), then immersed in a 1:2 mixture of sulfuric acid (H_2SO_4):hydrogen peroxide (H_2O_2) (volume: volume) (Piranha solution) for 30 minutes to clean organic residues off the surface. This was followed by a thorough rinse in water and then ethanol. The wafers were then spun dry in air.

In order to modify silicon wafers with octadecyltrimethoxysilane to provide a model hydrophobic surface a solution of toluene (25 mL), octylamine (1 drop) and octadecyltrimethoxysilane (0.5 mL) was prepared. The dried surfaces were immersed in this solution for 12 hours. Finally the surfaces were washed with water and then ethanol and spun dry.

A 5 mg/mL solution of PDMAEMA in dichloromethane was prepared and was filtered through a 0.2 μm filter. It was then added dropwise onto the surface until it was completely covered with the solution. The surface was then spun at 4000 rpm for 15 seconds.

The surfaces were treated with HHIC as described above for 180 s. The surfaces were then washed by immersion in a solution of CH_2Cl_2/NEt_3 95/5 overnight and then in an ultrasonic bath (Fisher Scientific Ultrasonicator, model FS20H) for 30 minutes. Finally they were rinsed with CH_2Cl_2 and then ethanol, and spun dry.

The quaternization of the cross-linked PDMAEMA surface was carried out by submerging it in acetonitrile (1 mL). Bromoethane (0.3 mL) was added and the surfaces were agitated at a rate of 20 rpm using a GyroTwister (Labnet International Inc.) overnight at room temperature. The surfaces were then rinsed well with acetonitrile and spun dry.

The antibacterial activities of the quaternized surfaces obtained against Gram-positive bacteria *Staphylococcus aureus* (*S. aureus* ATCC3307) and Gram-negative bacteria *Escherichia coli (E. coli* ATCC 29425*)* were studied using the antibacterial drop-test (4, 5) . *E. coli*/ *S. aureus*, precultured in 15 mL of nutrient broth (Difco™ BD) at 37° C for 24hr, were washed by centrifuging at 4000 rpm for 10min. After removing the supernatant, the cells were washed with phosphate buffer solution (PBS) twice and re-suspended and diluted to approximately 3×10^5 CFU/ml in PBS solution.

The samples were placed in sterilized Petri dishes. Then 100 μL of PBS solution with bacterial suspension was added drop-wise onto the surface of each sample and completely covered the sample surface. An uncoated substrate was used as a reference. The petri dishes were sealed and placed in an incubator at 37° C with the humidity 46%. After 3 h, the bacteria were washed from the surface of the sample by using 10 mL PBS in the sterilized Petri dish. From this solution, 100 μL was spread onto solid plate count agar (Difco™ BD). After incubation for 24hr at 37°C, the number of surviving bacterial colonies on the Petri dishes were counted. The results after multiplication with the dilution factor were expressed as mean colony forming units (CFU) per mL. The above experiments were carried out in triplicate for each sample. The percentage of

killed bacteria was calculated as ((CFU of initial bacterial suspension - CFUs of viable bacteria following surface contact)/CFU of initial bacterial suspension)*100. Results represent mean±SD of triplicates from three separate experiments ($P<0.05$).

Reducing protein adsorption via HHIC of PEO

Silicon wafers were purchased from University Wafer (Boston, USA). They were cut into small pieces (approximately 1.5 cm × 1.5 cm), then immersed in a 1:2 mixture of sulfuric acid (H_2SO_4):hydrogen peroxide (H_2O_2) (volume: volume) (Piranha solution) for 30 minutes to clean organic residues off the surface. This was followed by a thorough rinse in water and then ethanol. The wafers were then spun dry in air. Butyl rubber 402 was provided by LANXESS, Inc. Sarnia, Canada. Butyl rubber was purified by precipitation in toluene/acetone or by column chromatography before use. Poly(ethylene glycol) (PEO, MW = 100 000 g/mol) was purchased from Sigma-Aldrich. Rhodamine B, and fibrinogen (from human plasma) were purchased from Sigma-Aldrich. All chemicals were used without further purification.

To obtain epoxidized butyl ruber, butyl rubber 402 (11 g, 3.6 mmol of isoprene units) was first dissolved in dry toluene (300 mL). A previously dried solution of metachloroperoxybenzoic acid (6g in 180 mL) was added to the poly(isobutylene-co-isoprene) in solution. The resulting mixture was stirred overnight at room temperature. After evaporation of the solvent (*in vacuo*), epoxidized butyl rubber was purified by precipitation in acetone/toluene (2:1) twice. The resulting polymer (2) was dried under vacuum (yield 91%).
^{1}H NMR (400 MHz, benzene D6): δ 2.77 ppm (t, 1H, J = 3 Hz,, epoxide) 1.63 ppm (s, CH2 polyisobutylene), 1.30 ppm (s, CH3 polyisobutylene).

Thin films of butyl rubber were prepared by spin coating a solution of butyl rubber 402 in hexane (5 mg/mL, 100 μL for 1 cm^2, 6000 rpm, 30 s) on a clean silicon wafer. *Preparation of PEO coated butyl rubber surface*: Thin films of epoxidized butyl rubber were first prepared by spin-coating a solution of epoxidized butyl rubber (see above) in hexane (5 mg/mL, 100 μL for 1 cm^2, 6000 rpm, 30 s) on butyl coated silicon wafer after 30 s of HHIC treatment (see below). Thin films of PEO were then prepared by spin coating a solution of PEO in CH_2Cl_2 (4 mg/mL, 100 μL for 1 cm^2, 6000 rpm, 30 s) on an epoxidized butyl coated silicon wafer after 30 s of HHIC treatment. The resulting PEO film was also grafted by using HHIC for 100 s.

Rhodamine B 4-(3 hydroxypropyl) piperazine amide was prepared as previously described (6). To a round bottom flask charged with *N*, *N*'-disuccinimidyl carbonate (DSC) (1.8 mg, 7.0 μmol) and Rhodamine B 4-(3 hydroxypropyl)piperazine amide (1.8 mg, 3.2 μmol) was added 200 μL of distilled pyridine. After stirring at room temperature for 4 h, additional DSC (1.5 mg, 5.9 μmol) was added to achieve full conversion. After a total of 7 h, the resulting solution was immediately used to functionalize fibrinogen. To a solution of fibrinogen (10 mg, 0.030 μmol) in 5 mM phosphate buffer, pH 7.2 (6 mL) was added 40 μL (0.45 mg, 0.63 μmol) of the solution of Rhodamine B 4-(3-(N hydroxysuccinimidyloxocarbonyl)-propyl)piperazine amide. After stirring overnight at room temperature, the rhodamine-fibrinogen conjugate was purified by dialysis in 5 mM phosphate buffer, pH 7.2 for 2 days using a Spectra-Pore membrane with a molecular weight cut-off of 12-13 KDa. The buffer was changed 2 times.

A 400 μg/mL solution of the Rhodamine-fibrinogen conjugate in 5 mM phosphate buffer, pH 7.2 was prepared. The surfaces were then immersed in the protein solution. After 2 h, the non-adsorbed protein was removed by washing the surfaces with buffer and water. The fluorescence was then evaluated by using an LSM 510 multichannel point scanning confocal microscope (Laser 543 nm and band pass filter of 560-600 nm).

Monte Carlo (MC) model

The model implements a simple MC scheme for a collision cascade of hard-sphere particles of a mass $m = 2$ a.m.u. and a diameter of d = 2.92 Å (chosen to represent molecular hydrogen (7) in a cylindrical chamber of $L = 0.5$ *m* in length (the x coordinate is the cylinder axis) and D = 0.15 m in diameter (y and z coordinates). A series of uniform random numbers $u_i \in (0,1) \quad i = 1..5$ is used in the following procedure. The "initiator", i.e. a hyper-thermal particle(energy E = 100 - 1000 eV), with its velocity aligned along x, enters the chamber at the coordinate (0, $D\sqrt{u_1}\sin(2\pi u_2)$, $D\sqrt{u_1}\cos(2\pi u_2)$) and experiences a collision with the background gas of the same particles (not simulated explicitly) after having moved a free path l drawn from the exponential distribution $l = -\lambda \ln(u_3)$, where $\lambda = 1/n\sigma$ is the mean free path, $\sigma = \pi d^2$ is the hard sphere cross section, and $n = p/kT$ is the density of the background gas at the pressure p and temperature T = 293 K. This process results in the doubling of the number of particles, and is repeated for the following generations of the particles and the binary cascade of collisions is thus produced. The impact parameter $b = d\sqrt{u_4}$ and the azimuthal angle $\phi = 2\pi u_5$ for each collision are chosen randomly to render a uniform distribution of the target particle centres in the circle of the diameter 2d. All collisions (including the collisions of the particles with the walls of the chamber) are perfectly elastic and specular (momentum transfer occurs only in the direction normal to the collision surface). Those particles whose energy falls below $E < E_{cut}$ = 5 eV during the collision cascade, are discarded. All other particles with $E > E_{cut}$ = 5 eV, that reach the reaction zone at $x = L$, i.e. *the projectiles,* are counted. The initiator particle is discarded too if it reaches the reaction zone. The time is not included explicitly in the model, though it can be calculated. The *yield* is defined as the number of projectiles with an energy greater than the E_{cut}, produced per one initiator particle. Typically, we use 10 000 initiator particles to gather the statistics. The process described above results in the scale-free fragmentation of the incident energy and thus produces the power-law energy distributions for the projectiles.

***Ab initio* Molecular Dynamics (MD) calculations**

The simulation of collision processes were conducted with *ab initio* MD method (8). The microcanonical MD simulation was performed by integrating the classical Newton's equation of motion using Verlet algorithm (9). The time step has been set as 0.05 fs. At each time step, electronic energy and forces were calculated at B3LYP/6-31G* level (10) using Gaussian 03 package (11). The forces on each atom were then used for integrating the equation of motions.

Supplementary information text

Estimation of the C-H and C-C bond cleavage thresholds for both the molecular hydrogen and the atomic helium, used as hyperthermal projectiles.

The simplest formula for the energy fraction transferred from an incident hard-sphere particle of mass m_1, having initial energy E_1, to a target particle of mass m_2, initially at rest ($E_2 = 0$), during an absolutely elastic head-on collision, is the following:

$$\varepsilon = \frac{E_2^*}{E_1} = \frac{4m_1m_2}{(m_1+m_2)^2},$$

where the superscript * denotes the energy after collision. According to this formula, for H_2 projectiles, $\varepsilon = 0.89$ in a H_2/H collision and $\varepsilon = 0.49$ in a H_2/C collision. Consequently, since the energy transfer is more efficient for H_2 collisions with H, than for those with C, there is in principle a window of opportunity to do HHIC. Furthermore, the *ab-initio* simulations quoted in the main text indicate that about $E^*_2 \sim 8$ eV needs to be transferred during the collision to the internal energy of a hydrocarbon to cause the cleavage of both C-H and C-C bonds (they have comparable bond energies). Therefore, one can estimate the corresponding thresholds for E_1 as ~9 eV and ~16 eV, respectively, cleaving C-H and C-C bonds. Another estimation in the *ab-initio* simulation quoted in the main text can be given by subtracting the energy losses due to the energy transfer to the total kinetic energy of the molecule from the energy of the incident particle, which gives the thresholds of ~16 eV and ~30 eV for C-H and C-C bond breaking. These estimations should be compared to those quoted in the main text. Since there is a considerable disagreement between different estimations, we consider all the projectiles with the energies in the interval 5 eV to 40 eV as being capable to break a C-H bond, and we plot the relevant curves (such as those in Fig. 4b in the main text) for 5 eV, 19 eV, and 40 eV thresholds.

By contrast, for He projectiles, $\varepsilon = 0.64$ in a He/H collision and $\varepsilon = 0.75$ in a He/C collision. Since the latter figure is bigger than the former, the possibility to do HHIC with helium is hindered in principle as C-C bonds get broken on average more often than C-H bonds.

Estimation of the reaction rates and reaction collision cross-sections for HHIC and atomic hydrogen collision-induced dissociation CID.

As referred to in the main text, here we provide the calculations for the reaction rate and reaction collision cross section for HHIC, and compare them with the corresponding quantities of hydrogen abstraction by atomic hydrogen (12).

For a typical organic polymer of a density of ~1 g/cm^3 and of an average CH_2 composition (variation of the proportion of H does not significantly change the estimations below) the volume density of C atoms, *[C]*, can be estimated as ~4.3x10^{22} cm^{-3} and the corresponding area density is ~4.3x10^{16} cm^{-2}, for a ~10 nm thick polymer layer

First, let us consider the experiment (12), where an organic polymer has been cross-linked with the help of atomic H gas. The reaction of the abstraction of H from such polymer by an atomic

H˙ can be symbolically described as follows, $H\bullet + HCR \rightarrow \bullet CR + H_2$, where $\bullet$ denotes the radicals, and *R* stands for the rest of the polymer. This gives the reaction law:

$$-\frac{d[C]}{dt} = \frac{d[C\bullet]}{dt} = k[H][C] = k'[C],$$

where [C] can be expressed in either volume or area units. The absolute rate of the production of C radicals, $\frac{d[\bullet C]}{dt}$, can be estimated as $\frac{d[\bullet C]}{dt} \approx \frac{1\times10^{14} cm^{-2}}{100s} = 1\times10^{12} cm^{-2}s^{-1}$ (12), and the relatively high concentration of hydrogen atoms in the experiment (12) is $[H] \approx 1\times10^{15}\ cm^{-3}$. Therefore, the reaction rates are $k' = k[H] \approx 2.3\times10^{-5}\ s^{-1}$, and

$$k_{ref} \approx 2.3\times10^{-20}\ cm^3 s^{-1}. \quad (1)$$

where we denoted the reaction rate in the literature reference (12) with the subscript *ref*, as it is used as a reference value below.

By contrast, in the HHIC setup presented in this report, the concentration of the H_2 projectiles, *[H₂]*, is some 7 orders of magnitude lower (compared to the *[H]* quantity above). Indeed, at the H^+ plasma current of 10 mA, and other typical experimental conditions (as described in the main text), the typical flux of H_2 projectiles with energies in the range 5-40 eV is $j_{H_2} \approx 7\times10^{14}\ cm^{-2}s^{-1}$. This, at an average velocity of H_2 molecules, $\langle v \rangle \approx 4.4\times10^{6}\ cm/s$ (which would correspond to ~20 eV) gives a H_2 volume density of $[H_2] = j_{H_2}/\langle v \rangle \approx 1.5\times10^{8}\ cm^{-3}$.

Nevertheless, the reaction of hydrogen abstraction in the HHIC reactor proceeds some 100 times faster, that the one described above (12), even for the typical H_2 versus typical H concentrations in both experiments. What's more impressive, is that in terms of the reaction rate *k*, it is some 9 orders of magnitude faster!

Namely, the reaction in HHIC can be describes as $H_2(hyperthermal) + HCR \rightarrow \bullet CR + H_2 + H\bullet$, which gives following rate equation:

$$-\frac{d[C]}{dt} = \frac{d[\bullet C]}{dt} = k[H_2][C] = k'[C],$$

where the value for *[C]* is the same as above (taken for a typical organic layer) while one can estimate the absolute rate of the production of C radicals, $\frac{d[\bullet C]}{dt}$, as follows. We observe in our experiments, that for a typical flux of the H_2 projectiles $j_{H_2} \approx 7\times10^{14}\ cm^{-2}s^{-1}$, as indicated above, a ~10nm-thick layer of $C_{32}H_{66}$ can be cross-linked and rendered completely insoluble in ~10 seconds. Assuming that at least two C-H bonds per $C_{32}H_{66}$ molecule have to be cleaved in order to cross-link all $C_{32}H_{66}$ units into the insoluble film with at least one C-C cross-link per $C_{32}H_{66}$ unit, gives:

$\frac{d[\bullet C]}{dt} \approx \frac{4.3\times10^{16} cm^{-2}}{10s}\frac{2}{32} = 2.7\times10^{14} cm^{-2}s^{-1}$. Consequently, $k' = k[H_2] \approx 6.2\times10^{-3}\ s^{-1}$, and

$$k_{HHIC} \approx 4.2 \times 10^{-11}\ cm^3 s^{-1}. \quad (2)$$

More than nine orders of magnitude difference between the rates *k* in the cases of HHIC (Eq.2) and the literature case (12), (Eq. 1) can be explained simply as the temperature difference of the reactants H_2 and $H^{\bullet}$, respectively. Indeed, the barrier for the $H^{\bullet}$ abstraction (E_a~ *0.5* eV, (13)) should be compared with the temperature of hyperthermal H_2 (kT~20 eV) and to the room temperature of atomic $H^{\bullet}$ (kT~0.025 eV), in order to give the corresponding Boltzmann factors as follows: $\exp(-E_a/kT) \approx 0.97$ in the case of HHIC, and $\exp(-E_a/kT) \approx 2.1 \times 10^{-9}$ in the case of the literature example (12). Thus, HHIC is efficient simply because the reaction barriers are virtually unnoticeable for the swift hyperthermal projectiles!

The high efficiency of HHIC can be further clarified with some relevant collision data. First, HHIC is typically applied to the precursor molecules present as a condensed matter with an atomic areal density of one atom per ~5 $Å^2$ per atomic layer equivalent. Second, although the cross-section of dissociative collision of H_2 and a hydrocarbon is not known, once one knows the rate of the reaction *k* (Eq. 1 or Eq. 2), one can also estimate the corresponding reaction collision cross-section σ as follows. For the simple hard-spheres collision model of a gas phase reaction one obtains for the reaction rate *k*, (14):

$$k = \sigma \langle v \rangle \exp(-E_a/kT),$$

where $\langle v \rangle$ is an average velocity between the colliding particles and σ is the reaction collision cross-section. Substituting the values for HHIC, obtained above, into this expression one obtains $\sigma \sim 0.1\ A^2$.

Note, that the cross-section of the dissociative collision of He + H_2 is ~0.07 $Å^2$ at 10 eV (15) and that of $H^{\bullet}$ + CH_4 at 1.6 eV is 1.5 $Å^2$ (16), hence our estimation above is reasonable. If so, a hyperthermal H_2 projectile will penetrate the subsurface region and undergoes multiple scattering events in the top layer of a few nanometers before it loses enough energy and becomes non-reactive. In some of these scattering events, in addition to direct collision-induced C-H dissociation shown in Fig. 2 and movie S1, C-H dissociation can also proceed via hydrogen abstraction by atomic hydrogen generated due to the dissociation of H_2 during collision and due to the C-H dissociation. More importantly, both sources likely give hyperthermal atomic hydrogen. Since C-H dissociation via hydrogen abstraction is thermodynamically allowed and only has a small energy barrier E_a ~ 0.5 eV (13), C-H dissociation by hyperthermal atomic hydrogen can proceed readily even without any additional supply of thermal energy. This reaction channel, referred to as collision-assisted hydrogen abstraction herein, can effectively enhance the C-H dissociation yield, which is also supported by the high cross-section of hydrogen abstraction from hydrocarbon with hyperthermal atomic hydrogen (16).

Additional data

Table of Data Results for Figure 5

H^+ Extraction Energy (eV)	Thickness ratio of after:before HHIC (%)	Absolute Uncertainty (%)	Thickness ratio of after washing:before HHIC (%)	Absolute Uncertainty (%)
0	99	2	7	2
50	96	4	21	5
100	95	4	29	5
200	99	2	97	3
400	99	2	99	2

Thickness ratio for untreated and washed control sample is 6%.

Table of Data Results for Figure 6

Fluence (cm^{-2})	Young's Modulus (MPa)	Absolute Uncertainty (MPa)
0	1.26	0.21
$3.6x10^{14}$	1.94	0.40
$1.1x10^{15}$	2.13	0.74
$3.6x10^{15}$	2.40	1.05
$1.1x10^{16}$	2.71	0.71
$1.1x10^{17}$	7.06	1.33
$2.1x10^{17}$	9.83	1.92
$4.3x10^{17}$	14.03	2.71
$6.4x10^{17}$	18.68	3.68
$2.1x10^{18}$	18.56	3.52

Table of data for experiment comparing effects of hydrogen and helium in HHIC

	Thickness ratio for H_2 (%)	Thickness ratio for He (%)
after HHIC:before HHIC	97	76
after washing:before HHIC	96	76

References

1. G. Beamson, D. Briggs, *High Resolution XPS of Organic Polymers - The Scienta ESCA300 Database* (Wiley Interscience, 1992).
2. J. M. Hill, D. G. Royce, C. S. Fadley, L. F. Wagner, F. J. Grunthaner, *Chemical Physics Letters* **44**, 225 (1976).
3. W. Agut, D. Taton, S. Lecommandoux, *Macromolecules* **40**, 5653 (2007).
4. L. Cen, K. G. Neoh, E. T. Kang, *Langmuir* **19**, 10295 (2003).
5. J. H. Fu, J. Ji, W. Y. Yuan, J. C. Shen, *Biomaterials* **26**, 6684 (2005).
6. T. Nguyen, M. B. Francis, *Organic Letters* **5**, 3245 (2003).
7. G. A. Bird, *Molecular gas dynamics and the direct simulation of gas flows* (Clarendon Press ; Oxford University Press, Oxford; New York, 1998).
8. M. C. Payne, M. P. Tether, D. C. Allan, T. A. Arias, J. D. Joannopoulos, *Reviews of Modern Physics* **64**, 1045 (1992).
9. L. Verlet, *Physical Review Online Archive (Prola)* **159**, 98+ (1967).
10. A. D. Becke, *The Journal of Chemical Physics* **98**, 5648 (1993).
11. M. J. Frisch, *et al.*, Gaussian 03, Revision C.02. Gaussian, Inc., Wallingford, CT, 2004.
12. T. C. Sandreczki, I. M. Brown, *Macromolecules* **23**, 1979 (1990).
13. B. N. Kerkeni, D. C. Clary, *Physical Chemistry Chemical Physics* **8**, 917 (2006).
14. I. N. Levine, *Physical chemistry* (Boston : McGraw-Hill, 2002), fifth edn.
15. K. Sakimoto, *Journal of Chemical Physics* **112**, 5044 (2000).
16. G. J. Germann, Y.-D. Huh, J. J. Valentini, *The Journal of Chemical Physics* **96**, 5746 (1992).

Fig. S1 *Ab initio* molecular dynamics of 39 eV H_2 arriving with its molecular axis towards the C1-C2 bond of C_2H_6 and with H9 of H_2 hitting C2 of C_2H_6 (the respective views of H4 and H7 are blocked by H5 and H8) with 5 femtoseconds per step: After collision, the H_2 is scattered with a loss of about 18 eV in kinetic energy (44 % energy transfer) and a very small gain in vibrational and rotational energy. The C_2H_6 suffers no bond cleavage, with about 9 eV gain in kinetic energy and some gain in rotational/vibrational energy.

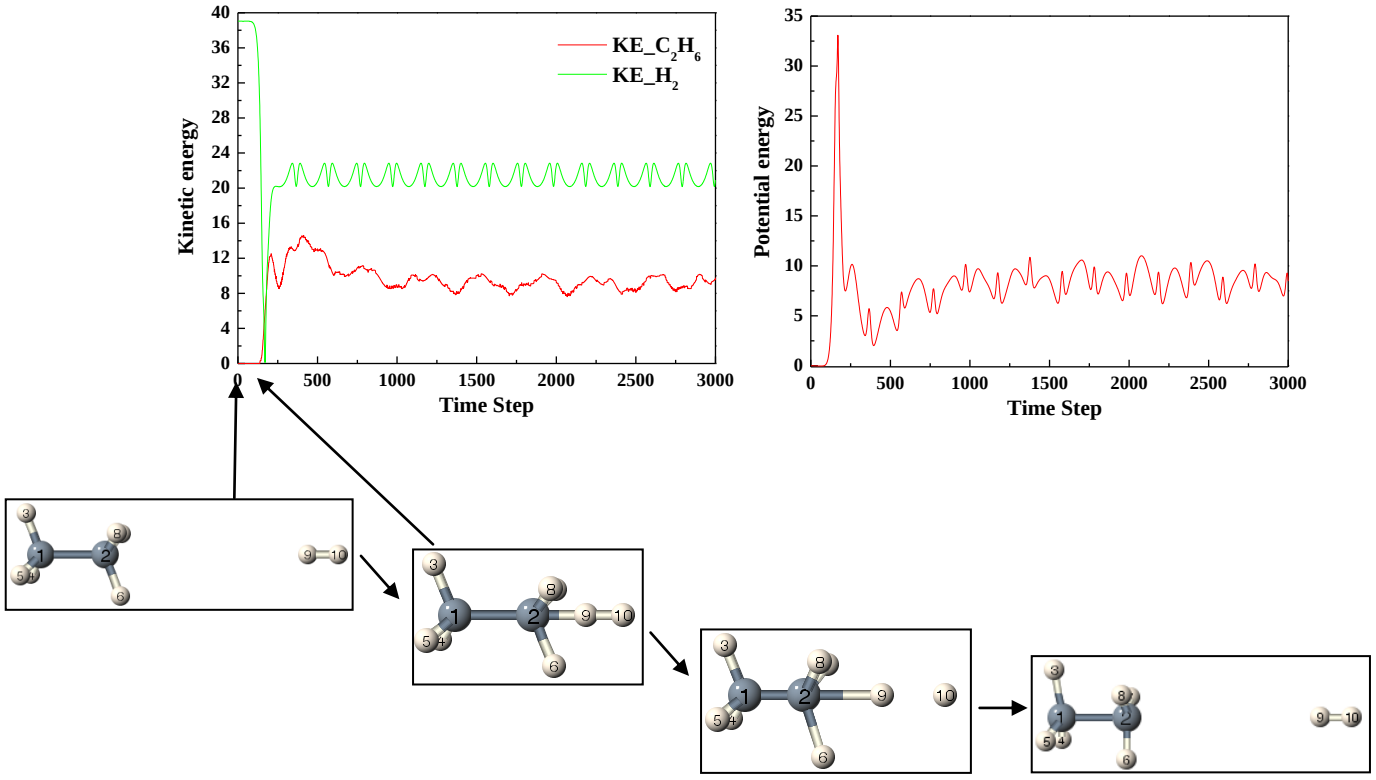

Movie S1 Molecular dynamics simulations of the collision event of 19 eV H_2 ---- hitting H-C of C_2H_6

Movie S2 Cascade collisions initiated by 400 eV H^+ in a background H_2 of 1 mTorr.